

# Exact-Exchange Density Functional Theory applied to a strongly inhomogeneous electron gas

S. Rigamonti, F. A. Reboredo\*, and C. R. Proetto

*Comisión Nacional de Energía Atómica  
Centro Atómico Bariloche and Instituto Balseiro  
8400 Bariloche, Argentina*

*\*Lawrence Livermore National Laboratory, Livermore, California 94550, USA*

## Abstract

A recently developed quasi two-dimensional exact-exchange formalism within the framework of Density Functional Theory has been applied to a strongly inhomogeneous interacting electron gas, and the results were compared with state-of-the-art Variational Quantum Monte Carlo (VMC) numerical simulations for a three-dimensional electron gas under a strong external potential. The VMC results, extremely demanding from the computational point of view, could be considered as a benchmark for the present theory. We observe a remarkable qualitative and quantitative agreement between both methods from the comparison of the exchange-hole densities, exchange-energy densities, and total exchange-energies per particle. This agreement is increasingly improved with the strength of the external potential when the electron gas becomes quasi-two-dimensional.

The search for accurate calculation schemes within the framework of Density Functional Theory (DFT) is of paramount importance in atomic, molecular, and solid state physics. [1] While DFT maps the problem of interacting inhomogeneous electron systems to a problem of effectively non-interacting inhomogeneous electrons, it provides no help in the determination of the exchange-correlation component of the total energy functional. [2,3] Largely, this obstacle has been overcome by using the so-called Local Density Approximation (LDA), which is based in the approximate equivalence in the long-wavelength limit between the inhomogeneous and homogeneous interacting electron gases, with the latter taken as a reference system. [4] The LDA (and generalized gradient corrections to the LDA, as the GGA) has been widely employed, however, even for strongly inhomogeneous systems, such as atoms and molecules, with surprisingly good results. [5] The application to strongly inhomogeneous solid state systems has been equally successful, [6] but some warnings raised quite recently when applied to two-dimensional electron gases (2DEG), [7] of the type formed at the interface between two semiconductors such as GaAs/Al<sub>x</sub>Ga<sub>1-x</sub>As. [8] Recently a study by Nekovee, Foulkes, and Needs (NFN) using Variational Quantum Monte Carlo (VMC) numerical simulations showed significant failures of the LDA and GGA in the description of the exchange hole of a 3D electron gas under the effect of a strong periodic potential. [9] Since plane wave expansions are a routine approach in DFT *ab-initio* codes NFN results call for methods that could describe accurately the electron gas in regions where the chemical bond is formed.

In this paper we present the first application of a recently developed quasi two-dimensional exact-exchange DFT (XX-DFT) method to a strongly inhomogeneous “metallic” system; we have found that this local exact exchange theory overcomes the problems presented by LDA and GGA. Previous application of the XX-DFT formalism includes atomic and molecular systems, [10] semiconductors (insulators), [11] and quasi 2DEG’s. [12] The method is distinguished from LDA, by avoiding the approximation of taking the exchange energy of the inhomogeneous electron gas as given by the exchange energy of the homogeneous electron gas, evaluated at the same (local) value of the density of the inhomogeneous system. Instead, the XX-DFT formalism uses the fact that the exchange energy is an explicit function of the *occupied* orbitals, [13] and exploit this to derive a local potential that minimizes a Kohn-Sham energy which includes the exchange energy exactly. [14] This elaborate treatment of the exchange potential, beyond the standard LDA-DFT scheme, was shown to be crucial in providing a theoretical explanation of striking experimental results in asymmetric semiconductor quantum wells. [12] These experiments and theoretical analysis suggest that the occupancy of a quantum well subbands proceed in an abrupt way, mediated by inter-subband exchange, the explanation being quite natural in the XX-DFT scheme.

The system under study is shown schematically in Fig. 1, and has been motivated by the recent analysis of a similar system by NFN using VMC numerical simulations; [9] the same system has been also studied by Rushton, Tozer, and Clark, [15] using the so-called Weighted Density Approximation (WDA), that treats both exchange and correlation in an approximate, but non-local, way. [16] Our model consists of a cosenoidal double well external potential  $V_{ext}(z) = V_0 \cos(qz)$ , which strongly modulates the electronic density along the  $z$  direction, but keeps the translational symmetry in the  $x - y$  plane; the system is ultimately confined by two infinite barriers located at  $z = \pm (d + \lambda)$ . The charge neutrality of the system was fulfilled by means of a positive jellium slab of uniform density  $\bar{n} = 3/4\pi r_s^3$ ,

where  $r_s = r_0/a_0$ , with  $4\pi r_0^3/3$  being the volume per electron, and  $a_0 = 0.529 \text{ \AA}$  the Bohr radius. Following Ref. (9),  $r_s$  was fixed at  $r_s = 2$ , while the amplitude  $V_0$  was chosen to be  $V_0 = 2.08\varepsilon_F^0$ , where  $\varepsilon_F^0$  is the Fermi energy corresponding to  $\bar{n}$ ; these values corresponds approximately to those of Al. We studied systems with three different modulations  $q$  of the external potential, corresponding to  $q_1 = 1.11k_F^0$ ,  $q_2 = 1.55k_F^0$ ,  $q_3 = 2.17k_F^0$ , with  $a_0k_F^0 = (3\pi^2\bar{n})^{1/3}$ . Note that in our model, decreasing  $q$  leads to an increasing  $\lambda$ , and consequently to increasingly smooth potentials (as the potential barrier height  $V_0$  is fixed), approaching the three-dimensional uniform situation.

Before starting with calculations, it is important to realize that  $\lambda = 2\pi/q \simeq 1 / k_F^0$ ; this leads to a strong quantization of the electronic degrees of freedom along  $z$ . Following the terminology of the quasi-2DEG's, we will denote as ‘‘subbands’’ each one of these quantized discrete levels. As electrons are free to move in the  $x - y$  plane, an in-plane parabolic dispersion relation is associated to each one of these subbands. To proceed, and exploiting the translational symmetry along the  $x - y$  plane (area  $A$ ), we propose as solutions of the three-dimensional Kohn-Sham (KS) equations  $\phi_{\nu\mathbf{k}\sigma}(\mathbf{r}) = \exp(i\mathbf{k} \cdot \rho)\xi_\nu^\sigma(z)/\sqrt{A}$ , with  $\mathbf{k}$  the in-plane wave vector,  $\rho$  the in-plane coordinate,  $\xi_\nu^\sigma(z)$  the subband wave function corresponding to an electron with a spin projection  $\sigma$  ( $\uparrow$  or  $\downarrow$ ) and subband index  $\nu$  ( $\nu = 0, 1, 2, \dots$ ). Proceeding with these solutions, the KS equations take the form of effective one-dimensional Schrödinger-like equations [17]

$$\left[ -\frac{1}{2} \frac{\partial^2}{\partial z^2} + V_{KS}(z, \sigma) \right] \xi_\nu^\sigma(z) = \varepsilon_\nu^\sigma \xi_\nu^\sigma(z), \quad (1)$$

with  $V_{KS}(z, \sigma)$  being the local KS spin-dependent potential, and  $\varepsilon_\nu^\sigma$  the eigenvalues.  $V_{KS}(z, \sigma)$  is the sum of several contributions

$$V_{KS}(z, \sigma) = V_{ext}(z) + V_H(z) + V_x^i(z, \sigma) + V_c(z, \sigma), \quad (2)$$

with  $V_H$ ,  $V_x^i$ , and  $V_c$  being the Hartree, exchange, and correlation contributions, respectively. The index  $i$  stands for the exact-exchange ( $i = XX$ ) or Local Density Approximation ( $i = LDA$ ). The Hartree potential is given by its classical expression,

$$V_H(z) = -2\pi \int_{-(\lambda+d)}^{\lambda+d} dz' |z - z'| [n(z') - n_{jell}(z')], \quad (3)$$

with  $n_{jell}(z) = \bar{n} \theta(\lambda + z)\theta(\lambda - z)$ , and  $\theta(x)$  being the step function ( $\theta(x) = 1$  if  $x > 0$ ,  $\theta(x) = 0$  if  $x < 0$ ). For  $V_c(z, \sigma)$  we follow the DFT prescription and define it through the functional derivative with respect to the density of the correlation contribution  $E_c$  to the total energy,

$$V_c(z, \sigma) = \frac{\delta E_c}{\delta n(z, \sigma)}, \quad (4)$$

and use LDA for its practical evaluation, using a recent parametrization of the correlation energy per particle for the interacting homogeneous electron gas by Gori-Giorgi, Sacchetti, and Bachelet. [18] In equations above,  $n(z)$  is the zero-temperature *three-dimensional* electron density

$$n(z) = \sum_{\sigma} n(z, \sigma) = \frac{1}{4\pi} \sum_{\nu\sigma} (k_F^{\nu\sigma})^2 |\xi_{\nu}^{\sigma}(z)|^2, \quad (5)$$

$n(z, \sigma)$  being the fraction of  $\sigma$  polarized electrons.  $\mu$  is the chemical potential (or Fermi level) of the system, which is determined by the electrostatic and thermodynamic equilibrium with a reservoir, and  $k_F^{\nu\sigma} = \sqrt{2(\mu - \varepsilon_{\nu}^{\sigma})\theta(\mu - \varepsilon_{\nu}^{\sigma})}$ . It remains to define  $V_x^{XX}(z)$ . As explained above, we avoid its usual local (LDA), or semilocal (GGA) expressions, using instead the recently developed XX-DFT formalism. [10,11] As shown elsewhere, [12] the exact-exchange potential for our quasi two-dimensional geometry is defined by the equation

$$V_x^{XX}(z, \sigma) = \frac{\delta E_x}{\delta n(z, \sigma)} = A \sum_{\nu} \int dz' \left\{ \int dz'' \left[ \frac{\delta E_x}{\delta \xi_{\nu}^{\sigma}(z'')} \frac{\delta \xi_{\nu}^{\sigma}(z'')}{\delta V_{KS}(z', \sigma)} + c.c. \right] + \left[ \frac{\delta E_x}{\delta k_F^{\nu\sigma}} \frac{\delta k_F^{\nu\sigma}}{\delta V_{KS}(z', \sigma)} \right] \right\} \frac{\delta V_{KS}(z', \sigma)}{\delta n(z, \sigma)}. \quad (6)$$

In equation above, the functional derivatives  $\delta E_x / \delta \xi_{\nu}^{\sigma}(z)$  and  $\delta E_x / \delta k_F^{\nu\sigma}$  can be evaluated directly from the explicit expression for the exchange energy  $E_x$  in terms of  $\xi_{\nu}^{\sigma}(z)$  and  $k_F^{\nu\sigma}$ .  $\delta \xi_{\nu}^{\sigma}(z) / \delta V_{KS}(z', \sigma)$  and  $\delta k_F^{\nu\sigma} / \delta V_{KS}(z, \sigma)$  are evaluated using first-order perturbation theory from Eq. (1). Finally,  $\chi_{\sigma}^{-1}(z, z') \equiv \delta V_{KS}(z', \sigma) / \delta n(z, \sigma)$  is the inverse of the operator  $\chi_{\sigma}(z, z') \equiv \delta n(z, \sigma) / \delta V_{KS}(z', \sigma)$  given by

$$\chi_{\sigma}(z, z') = \frac{1}{2\pi A} \sum_{\nu}^{\text{occ}} \left[ \sum_{\nu'(\neq\nu)} (k_F^{\nu\sigma})^2 \frac{\xi_{\nu}^{\sigma}(z) \xi_{\nu'}^{\sigma}(z) \xi_{\nu'}^{\sigma}(z') \xi_{\nu}^{\sigma}(z')}{\varepsilon_{\nu}^{\sigma} - \varepsilon_{\nu'}^{\sigma}} - [\xi_{\nu}^{\sigma}(z) \xi_{\nu}^{\sigma}(z')]^2 \right]. \quad (7)$$

The first term in Eq. (7) comes from first-order perturbation theory [11], whereas the second term results from first-order perturbation theory and the thermodynamic equilibrium between the electronic system and the reservoir that fixes a common chemical potential  $\mu$  allowing (in principle) the change of the number of particles. [19] Indeed, without the reservoir, the operator  $\chi_{\sigma}(z, z')$  in general cannot be inverted because it is singular [11]. The alternative to  $V_x^{XX}(z)$  is the widely employed  $V_x^{LDA}(z)$ , defined as

$$V_x^{LDA}(z, \sigma) = - \left[ \frac{6n(z, \sigma)}{\pi} \right]^{1/3}. \quad (8)$$

As it is well known, Eq.(1), together with Eqs.(3), (4), and (6) for XX-DFT, or (7) for LDA-DFT should be solved iteratively in a self-consistent way. All results denoted as XX (LDA) in what follows have been obtained by performing this numerical self-consistent procedure with  $V_x^{XX}(z)$  ( $V_x^{LDA}(z)$ ) inserted in Eq.(1), and by assuming a paramagnetic situation for the present high-density metallic system. Using as input the set of parameters defined above, the output of this self-consistent calculation correspond to a situation with two (four, counting spin) occupied subbands ( $\nu = 0, 1$ ) for the three different modulations  $q/k_F^0$ .

One way to characterize the accuracy of a many-body approach, is to analyze the exchange-correlation hole density, in terms of which the exchange-correlation energy could be defined. As the emphasis of the present work is on exchange effects, we will restrict our analysis mainly to the exchange-hole density. We start from the exact expression for the exchange-hole density, [20]

$$h_x(\mathbf{r}, \mathbf{r} + \mathbf{R}) \equiv -\frac{1}{2} \frac{|\rho(\mathbf{r}, \mathbf{r} + \mathbf{R})|^2}{n(\mathbf{r})}, \quad (9)$$

where

$$\rho(\mathbf{r}, \mathbf{r} + \mathbf{R}) \equiv \sum_{\nu\mathbf{k}\sigma} \theta[\mu - \varepsilon_\nu^\sigma(\mathbf{k})] \phi_{\nu\mathbf{k}\sigma}^*(\mathbf{r} + \mathbf{R}) \phi_{\nu\mathbf{k}\sigma}(\mathbf{r}) \quad (10)$$

is the density matrix associated to our problem.  $\varepsilon_\nu^\sigma(\mathbf{k}) = \varepsilon_\nu^\sigma + (\hbar\mathbf{k})^2/2m$  and note that  $\rho(\mathbf{r}, \mathbf{r}) = n(\mathbf{r})$ . The physical meaning of  $h_x(\mathbf{r}, \mathbf{r} + \mathbf{R})$  is that it represents the density of the exchange hole at point  $\mathbf{r} + \mathbf{R}$  (observational point) due to the presence of an electron (test particle) located at  $\mathbf{r}$ . Evaluating Eq.(9) in our quasi two-dimensional geometry of Fig. 1, we obtain

$$h_x(\mathbf{r}, \mathbf{r} + \mathbf{R}) = -\frac{1}{2(\pi R_{||})^2 n(z)} \sum_{\nu, \nu'} k_F^\nu k_F^{\nu'} J_1(k_F^\nu R_{||}) J_1(k_F^{\nu'} R_{||}) \xi_\nu^*(z + Z) \xi_\nu(z) \xi_{\nu'}(z + Z) \xi_{\nu'}^*(z), \quad (11)$$

where  $\mathbf{R} = (R_{||}, Z)$ , and  $J_1(x)$  is the first-order cylindrical Bessel function. [21] Taking the limit  $R_{||}, Z \rightarrow 0$ , it is easy to check that  $h_x(\mathbf{r}, \mathbf{r}) = -n(\mathbf{r})/2$ , and by explicit integration the fulfillment of the exact constraint [20]

$$\int d\mathbf{R} h_x(\mathbf{r}, \mathbf{r} + \mathbf{R}) = -1, \quad (12)$$

is immediate. In Eq.(11), it is interesting to note, first, the absence of the in-plane coordinate  $\rho$  corresponding to the test particle, which result from the translational symmetry in the  $x - y$  plane; choosing  $\rho = 0$  without any loss in generality,  $h_x(\mathbf{r}, \mathbf{r} + \mathbf{R})$  could be equally written as  $h_x(z; z + Z, R_{||})$ . Second, the dependence of  $h_x$  only on the magnitude of  $R_{||}$  means that the exchange hole has cylindrical symmetry along the  $z$  axis. Third, integration of  $n(z) \times h_x(z; z + Z, R_{||})/R$  ( $R = |\mathbf{R}|$ ) in  $z, Z$ , and  $R_{||}$  leads exactly to the definition of the exchange energy used to derive  $V_x^{XX}(z)$  in Eq.(6). In the limit  $k_F^\nu R_{||} \gg 1$  (assuming a finite occupancy of all occupied subbands), and using the asymptotic expansion of the Bessel function, we obtain

$$h_x(\mathbf{r}, \mathbf{r} + \mathbf{R}) \simeq -\frac{1}{(\pi R_{||})^3 n(\mathbf{r})} \times \sum_{\nu, \nu'} \sqrt{k_F^\nu k_F^{\nu'}} \cos(k_F^\nu R_{||} - \frac{3\pi}{4}) \cos(k_F^{\nu'} R_{||} - \frac{3\pi}{4}) \xi_\nu^*(z + Z) \xi_\nu(z) \xi_{\nu'}(z + Z) \xi_{\nu'}^*(z). \quad (13)$$

From Eq. (13), is evident that the asymptotic behavior of  $h_x(\mathbf{r}, \mathbf{r} + \mathbf{R})$  is given by  $R_{||}^{-3}$  along the  $x - y$  plane; on the other side, the decay along  $z$  is controlled by the extent of the subband wave-functions  $\xi_\nu(z)$ . In what follows, we will denote by  $h_x^{XX}(\mathbf{r}, \mathbf{r} + \mathbf{R})$  the exchange-hole density as given by Eq.(11), evaluated with the self-consistent subband wavefunctions  $\xi_\nu(z)$  that are the solutions of Eq.(1) with  $V_x^{XX}(z)$ . On the other side, evaluation of Eq.(9) in the LDA-DFT scheme using 3D plane waves yields

$$h_x^{LDA}(\mathbf{r}, \mathbf{r} + \mathbf{R}) = -\frac{n(\mathbf{r})}{2} F[k_F(\mathbf{r})R], \quad (14)$$

with  $F(x) = 9[(\sin x - x \cos x)/x^3]^2$ . In Eq.(14), and according to the LDA prescription  $k_F(\mathbf{r}) = [3\pi^2 n(\mathbf{r})]^{1/3}$ . We will denote by  $h_x^{LDA}(\mathbf{r}, \mathbf{r} + \mathbf{R})$  the exchange-hole density as given by Eq.(14), evaluated with the self-consistent subband wavefunctions  $\xi_\nu(z)$  that are the solutions of Eq.(1) with  $V_x^{LDA}(z)$ . It is easy to see that  $F(x) \rightarrow 1$  for  $x \rightarrow 0$ , while it decays as  $x^{-4}$  for  $x = k_F(\mathbf{r})R \gg 1$ . This simple dependence of  $F(x)$  on  $x$  implies that  $h_x^{LDA}$  is *always* centered on the electron coordinate  $\mathbf{r}$ . Besides, it is clear that  $h_x^{LDA}(\mathbf{r}, \mathbf{r} + \mathbf{R})$  is a spherically symmetric function of  $\mathbf{R}$ , and centered at  $\mathbf{r}$ .

Fig. 2 allows a qualitative comparison of both holes at a density maximum, corresponding to the electron coordinate  $\rho = 0$ ,  $z = -\lambda/2$  being located at the left potential well of Fig. 1. For this case, both holes are centered at the electron coordinate. Note that for both upper and lower panels, only half of the exchange hole has been represented; the full hole could be obtained by reflection with respect to the  $z$  axis. The exact-exchange hole is contracted along the confinement direction, due to the fact allowed above that the decay along the  $x - y$  plane and along the  $z$  direction are different, as seen explicitly from Eq. (13). The fact that  $h_x^{XX}(\mathbf{r}, \mathbf{r} + \mathbf{R})$  has essentially zero strength at the right well minima, simply means that the system is in the “atomic” or isolated well limit, with a very small amount of tunneling or subband wave-function overlap between the two wells. It is also interesting to note the Friedel-like oscillations of the exact-exchange and LDA holes, each of them reflecting the different types of symmetry of the corresponding holes.

The situation displayed in Fig. 3, corresponding to the electron coordinate  $\rho = 0$ ,  $z = 0$  at the density minimum, is strikingly different, compared with Fig. 2. Here,  $h_x^{XX}(\mathbf{r}, \mathbf{r} + \mathbf{R})$  attains its maximum strength when the observational coordinate  $Z$  coincides with the density maximum ( $z = \pm\lambda/2$ ). This is the physically correct behavior that one expects for the exchange-hole density, and that can easily be obtained from Eq.(11): Restricting for simplicity the analysis to the case where only one subband ( $\nu = 0$ ) is occupied, this equation simplifies to

$$h_x^{XX}(\mathbf{r}, \mathbf{r} + \mathbf{R}) = -\frac{[J_1(k_F^0 R_0)]^2}{\pi R_0^2} [\xi_0(z + Z)]^2, \quad (15)$$

which clearly attains its maximum strength, as a function of  $Z$ , when the argument of the subband wave function ( $z + Z$ ) coincides with a density maximum. This non-local behavior of the exact-exchange hole is clearly preserved when more than one subband is occupied (two subbands are occupied for the situation displayed in Figs. 2, 3, and 4). For  $z = \pm\lambda/2$  (Fig. 2) this happens for  $Z = 0$ , while for  $z = 0$ , this happens for  $Z = \pm\lambda/2$ . The LDA exchange hole, on the other side, is centered at the electron coordinate  $z$ . Attention should be paid also to the quantitative values of  $h_x^{XX}(\mathbf{r}, \mathbf{r} + \mathbf{R})$  and  $h_x^{LDA}(\mathbf{r}, \mathbf{r} + \mathbf{R})$  in Fig. 3. In the exact-exchange case,  $h_x^{XX}$  has a maximum strength value of about half of its value in Fig. 2, which is reasonable keeping in mind the constraint given by Eq.(12). On the other side,  $h_x^{LDA}$  has a maximum strength of about two orders of magnitude smaller than  $h_x^{XX}$ , and accordingly it has an “anomalous” large extent in real space in order to satisfy Eq. (12). Note also that the extent in real space for  $h_x^{XX}(\mathbf{r}, \mathbf{r} + \mathbf{R})$  is similar in Figs. 2 and 3, as it should be, as in this case and for both situations the size of the hole is dictated by the accumulation points of electronic density.

We show in Fig. 4 the exchange-energy densities differences, defined as follows:  $\Delta e_x^{VMC}(z) = e_x^{XX}(z) - e_x^{VMC}(z)$  (full thick line), and  $\Delta e_x^{LDA}(z) = e_x^{XX}(z) - e_x^{LDA}(z)$  (dashed thick line). Exchange-energy densities are obtained from

$$e_x^i(\mathbf{r}) = \frac{1}{2} \int \frac{d\mathbf{R}}{R} n(\mathbf{r}) h_x^i(\mathbf{r}, \mathbf{r} + \mathbf{R}) \quad (16)$$

with  $i = XX, LDA$ . The full thin line corresponds to the XX density  $n^{XX}(z)$ , the dotted thin line to the VMC density  $n^{VMC}(z)$ . We will discuss first the comparison between XX and VMC calculations. While in principle both methods give an exact treatment to the exchange-energy, and accordingly they should coincide, in practice there are three possible sources for the small differences observed in Fig. 4: *i*) while our double quantum well system is a very good approximation to the periodic system studied by NFN, the equivalence is not perfect from the “model” point of view, [22] *ii*) even if both models were identical, for the practical implementation of the VMC calculation, the external potential  $V_{ext}(z)$  used by NFN is not identical of ours (although it should be close to it), and *iii*) even if both the model *and* the external potential were identical, still we are treating correlation at the LDA level, while NFN treats correlation with VMC accuracy, presumably a much better approximation than LDA, and definitively quite different. As a consequence of these three factors, small differences between the two different densities profiles result, which in turn translate to the small differences for the exchange-energy densities observed in Fig. 4. It is important to realize, however, that points *i* and *ii* above are just consequence of the different scheme of calculations, while point *iii* is the important and intrinsic difference between XX-DFT and VMC. It is also interesting to note that the differences between XX and VMC are mainly concentrated in regions of high density, as expected; besides, differences increase from top (small  $q$ ) to bottom (large  $q$ ), as both models increasingly disagree in the large  $q$  limit. While from the results presented in Table I for the corresponding integrated magnitudes the difference between XX and VMC is smallest for the intermediate case  $q/k_F^0 = 1.55$ , from Fig. 4 it is clear that this is due to an (accidental) error cancellation. Based in the almost perfect agreement between  $n^{XX}(z)$  and  $n^{VMC}(z)$  displayed in Fig. 4 for  $q/k_F^0 = 1.11$ , it is clear that our modelization of the periodic system studied by NFN is at best in this quasi two-dimensional limit (see below). It is then plausible to assume that the remaining discrepancy between XX and VMC is mainly due to the different treatment of correlation in both cases. In this context, it is interesting to point out that in our case, the correlation energy per particle is typically 15 % of the exchange-correlation energy per particle. The comparison between XX and LDA exchange-energy densities shows large local deviations between the two methods, the amplitude of the differences being about a factor of two greater than between XX and VMC.

The situation is similar for the differences in the integrated energies presented in Table I, the differences between XX and VMC being much smaller than between XX and LDA for  $q/k_F^0 = 1.11$  and 1.57. The difference between XX and LDA exchange energies (per particle) is smaller than between XX and VMC for  $q/k_F^0 = 2.17$ . As can be seen from Fig. 4, this is in part due to a large error cancellation of the LDA results, which, being non-systematic is difficult to control, and also due to the fact that as  $q$  increases, our model and the NFN model move towards different limits (see below).

We show in Fig. 5 the exchange energy per particle  $\varepsilon_x$ , calculated in different approximations, as a function of the potential modulation  $q/k_F^0$ . In order to place these results in

perspective, it is important to note that the exchange energy per particle for the homogeneous 3D electron gas is

$$\varepsilon_x^{3D}(r_s) = -\frac{3}{4\pi} \left(\frac{9\pi}{4}\right)^{1/3} \frac{1}{r_s}, \quad (17)$$

while for a 2D homogeneous electron gas it is

$$\varepsilon_x^{2D}(r_s) = -\frac{4\sqrt{2}}{3\pi} \frac{1}{r_s}. \quad (18)$$

For  $r_s = 2$ , we obtain  $\varepsilon_x^{3D}(r_s = 2) \simeq -0.23$ ,  $\varepsilon_x^{2D}(r_s = 2) \simeq -0.30$ . For  $q/k_F^0 \rightarrow 0$ , the system resembles a three-dimensional uniform electron gas, which explains the decreasing (in absolute value) of the exchange energy for  $q/k_F^0 \lesssim 1$ . While our XX-DFT formalism is ideally suited for the study of strongly inhomogeneous systems, it is numerically inefficient for reaching the 3D limit, when a large number of subbands become occupied and the (numerical) calculation becomes increasingly cumbersome. [24] The tendency of the exchange energy towards the homogeneous 3D limit  $\varepsilon_x^{3D}(2) \simeq -0.23$  is however clearly displayed in Fig. 5. It is also interesting to note how LDA becomes an increasingly better approximation to XX for  $q/k_F^0 \rightarrow 0$ , as one expects. The opposite limit  $q/k_F^0 \gtrsim 1$  is also worth analyzing. In this case, the periodic model studied by NFN becomes increasingly three-dimensional, as the fixed-height barriers become thinner and electrons are increasingly able to tunnel through them. Our model, on the other side, in the limit  $q/k_F^0 \gtrsim 1$ , and as a consequence of the constraint  $\lambda = 2\pi/q$ , departs from the NFN model and becomes more similar to an infinite barrier quantum well of width  $2d$  with a positively charged layer at its center. The different limits reached by the model of NFN and ours explains the progressive disagreement between XX and VMC which is seen for  $q/k_F^0 \gtrsim 2$ . Besides these two limiting features, clearly the more interesting region is the intermediate regime about  $q/k_F^0 \simeq 1$ , where the inhomogeneity reaches its maximum strength. The proximity of the  $\varepsilon_x^{XX}$  and  $\varepsilon_x^{VMC}$  to the 2D value  $\varepsilon_x^{2D}(2) \simeq -0.30$  tells us that for  $q/k_F^0 \simeq 1$  the system is quite close to the strict two-dimensional limit. Quite good agreement is observed between XX and VMC in this strongly inhomogeneous regime, as according to Table I, the percentage error between both calculations is about 0.65 %. This should be compared with the corresponding error between XX and (our) LDA, that reaches a value of about 2.4 % in the same quasi two-dimensional regime, almost four times higher.

In summary, we have checked the accuracy of the exact-exchange density functional method as applied to a strongly inhomogeneous interacting electron gas, and compared with the best available results. We have analyzed the exact-exchange hole density, and found that it is strongly non-local when evaluated in regions of low-density. From the comparison with the results of Variational Quantum Monte Carlo, we found a remaining discrepancy of about 0.65 % between the exact-exchange and VMC exchange contributions, that we attribute to the different treatment of correlation in both approaches. Exact-Exchange Density Functional Theory works at best in the worse case for LDA, that is, when the strongly inhomogeneous electron gas is closer to the quasi two-dimensional limit. Our results motivate the urge for better and more accurate correlation functionals, and work in this direction is in progress.



The authors are very grateful to the authors of Ref.(9), who provides the data on their VMC calculations displayed in Fig. 4 prior to publication and for useful comments, and to K. Hallberg for a critical reading of the manuscript. We also benefited from the code provided by the authors of Ref.(18) for the calculation of the correlation energy per particle. S.R. acknowledges support from the Instituto Balseiro of S. C. de Bariloche, and F.A.R. and C.R.P. are indebted to CONICET of Argentina for financial support.

## REFERENCES

- [1] R. G. Parr and W. Yang, in *Density-Functional Theory of Atoms and Molecules* (Oxford University Press, New York, 1989); R. O. Jones and O. Gunnarsson, *Rev. Mod. Phys.* **61**, 689 (1989); W. Kohn, in *Nobel Lecture: Electronic structure of matter - wave functions and density functionals*. *Rev. Mod. Phys.* **71**, 1253 (1999).
- [2] P. Hohenberg and W. Kohn, *Phys. Rev.* **136**, B864 (1964).
- [3] W. Kohn and L. J. Sham, *Phys. Rev.* **140**, A1133 (1965).
- [4] W. Kohn and P. Vashishta, in *Theory of the Inhomogeneous Electron Gas*, edited by S. Lundqvist and N. H. March (Plenum, New York, 1983).
- [5] A. R. Williams and U. Von Barth, in *Theory of the Inhomogeneous Electron Gas*, edited by S. Lundqvist and N. H. March (Plenum, New York, 1983).
- [6] T. Ando, A. B. Fowler, and F. Stern, *Rev. Mod. Phys.* **54**, 437 (1982).
- [7] Y.-H. Kim, I.-H. Lee, S. Nagaraja, J. P. Leburton, R. Q. Hood, and R. M. Martin, *Phys. Rev. B* **61**, 5202 (2000); L. Pollack and J. P. Perdew, *J. Phys.: Condens. Matter* **12**, 1239 (2000); P. García-González, *Phys. Rev. B* **62**, 2321 (2000); P. García-Gonzalez and R. W. Godby, *Phys. Rev. Lett.* **88**, 056406 (2002).
- [8] G. Bastard, in *Wave mechanics applied to semiconductor heterostructures* (Les Ulis: Les éditions de Physique, 1988).
- [9] M. Nekovee, W. M. C. Foulkes, and R. J. Needs, *Phys. Rev. Lett.* **87**, 036401 (2001).
- [10] J. B. Krieger, Y. Li, and G. J. Iafrate, *Phys. Rev. A* **45**, 101 (1992); S. Ivanov, S. Hirata, and R. Bartlett, *Phys. Rev. Lett.* **83**, 5455 (1999); A. Görling, *Phys. Rev. Lett.* **83**, 5459 (1999); F. Della Sala and A. Görling, *Phys. Rev. Lett.* **89**, 033003 (2002).
- [11] M. Städele, J. A. Majewski, P. Volg, and A. Görling, *Phys. Rev. Lett.* **79**, 2089 (1997); M. Städele, M. Moukara, J. A. Majewski, P. Volg, and A. Görling, *Phys. Rev. B* **59**, 10031 (1999).
- [12] A. R. Goñi, U. Haboeck, C. Thomsen, K. Ebert, F. A. Reboredo, C. R. Proetto, and F. Guinea, *Phys. Rev. B* **65**, 121313(R); P. Guidici, A. R. Goñi, U. Haboeck, C. Thomsen, K. Ebert, F. A. Reboredo, and C. R. Proetto, *Proceedings of the ICPS 26*; F. A. Reboredo and C. R. Proetto, (submitted to *Phys. Rev. Lett.*).
- [13] V. Sahni, J. Gruenbaum, and J. P. Perdew, *Phys. Rev. B* **26**, 4371 (1982).
- [14] A. Görling and M. Levy, *Phys. Rev. B* **47**, 13105 (1993); A. Görling and M. Levy, *Phys. Rev. A* **50**, 196 (1994).
- [15] P. P. Rushton, D. J. Tozer, and S. J. Clark, *Phys. Rev. B* **65**, 193106 (2002).
- [16] O. Gunnarsson, M. Jonson, and B. I. Lundqvist, *Phys. Rev. B* **20**, 3136 (1979).
- [17] Hartree (atomic) units are used in this work:  $a_0 = \hbar^2/me^2 \simeq 0.529 \text{ \AA}$  is the unit of length,  $\hbar^2/ma_0^2 \simeq 27.2 \text{ eV}$  is the unit of energy.
- [18] P. Gori-Giorgi, F. Sacchetti, and G. B. Bachelet, *Physical Review B* **61**, 7353 (2000).
- [19] In the present work all results are for a fixed number of particles. From the numerical point of view, however, it is more convenient to treat the model in Fig. 1 as an open system in contact with a particle bath at chemical potential  $\mu$ . To satisfy the constraint of constant number of particles, the chemical potential  $\mu$  is then adjusted at each iteration of the self-consistent calculation loop.
- [20] O. Gunnarsson and B. I. Lundqvist, *Phys. Rev. B* **13**, 4274 (1976); J. P. Perdew and A. Zunger, *Phys. Rev. B* **23**, 5048 (1981).
- [21] W. Kohn and A. E. Mattsson, *Phys. Rev. Lett.* **81**, 3487 (1998). These authors have

obtained a related expression for the inverse radius of the exchange hole, which is basically the integral over all  $\mathbf{R}$  of  $h_x(\mathbf{r}, \mathbf{r} + \mathbf{R})$ , weighted with  $R^{-1}$ .

- [22] For example, while the *average* density  $\bar{n}$  is the same in the NFN model and ours, locally the electrons are distributed in slightly different ways: between  $-\lambda \leq z \leq \lambda$  (and periodically) in the first case, between  $-(d + \lambda) \leq z \leq d + \lambda$  in the present case. The difference in boundary conditions at  $z = \pm\lambda$  between the periodic model and ours is the source of the differences between  $n^{XX}(z)$  and  $n^{VMC}(z)$  observed for  $|z| \simeq \lambda$ , and whose importance increases from top to bottom.
- [23] M. Nekovee, W. M. C. Foulkes, and R. J. Needs (unpublished).
- [24] Two subbands are occupied in the range  $1 \lesssim q/k_F^0 \lesssim 3$ ; moving towards the long wavelength limit, the number of occupied subbands progressively increases from two to eight in the range  $0.5 \lesssim q/k_F^0 \lesssim 1$ .

## FIGURES

FIG. 1. Schematic representation of the external potential  $V_{ext}(z) = V_0 \cos(qz)$ . The wave-length of the modulation is  $\lambda = 2\pi/q$ , and the amplitude  $V_0 = 2.08 \varepsilon_F^0$ .  $d = 2 a_0 \simeq 1$  A is the distance between the end of the jellium slab (shaded region) and the infinite potential barriers located at  $z = \pm(d + \lambda)$ .

FIG. 2. Exchange-hole density at a density maximum ( $z = -\lambda/2$  in Fig. 1), for  $q/k_F^0 = 1.11$ . Upper panel:  $h_x^{XX}(\mathbf{r}, \mathbf{r} + \mathbf{R})$ . Lower panel:  $h_x^{LDA}(\mathbf{r}, \mathbf{r} + \mathbf{R})$ .

FIG. 3. Exchange-hole density at a density minimum ( $z = 0$  in Fig. 1), for  $q/k_F^0 = 1.11$ . Upper panel:  $h_x^{XX}(\mathbf{r}, \mathbf{r} + \mathbf{R})$ . Lower panel:  $h_x^{LDA}(\mathbf{r}, \mathbf{r} + \mathbf{R})$ . It is important to realize that the numerical value of  $h_x^{LDA}$  at its point of *maximum* strength coincides with the value of  $h_x^{XX}$  at its point of *minimum* strength, marked with a square full dot.

FIG. 4. Left-scale, full (dashed) thick line: Difference between XX and VMC (LDA) exchange-energy densities  $\Delta e_x^{VMC}(z) = e_x^{XX}(z) - e_x^{VMC}(z)$  ( $e_x^{XX}(z) - e_x^{LDA}(z)$ ), versus position in the system, and for the three modulations. Right-scale: exact-exchange (full thin line) and VMC (dotted thin line) electronic densities  $n^{XX}(z)$  and  $n^{VMC}(z)$ , respectively; note that both sets of densities are almost indistinguishable except for  $q/k_F^0 = 2.17$  and  $|z| \simeq \lambda$ . Data corresponding to  $e_x^{VMC}(z)$  and  $n^{VMC}(z)$  provided by the authors of Ref.(23).

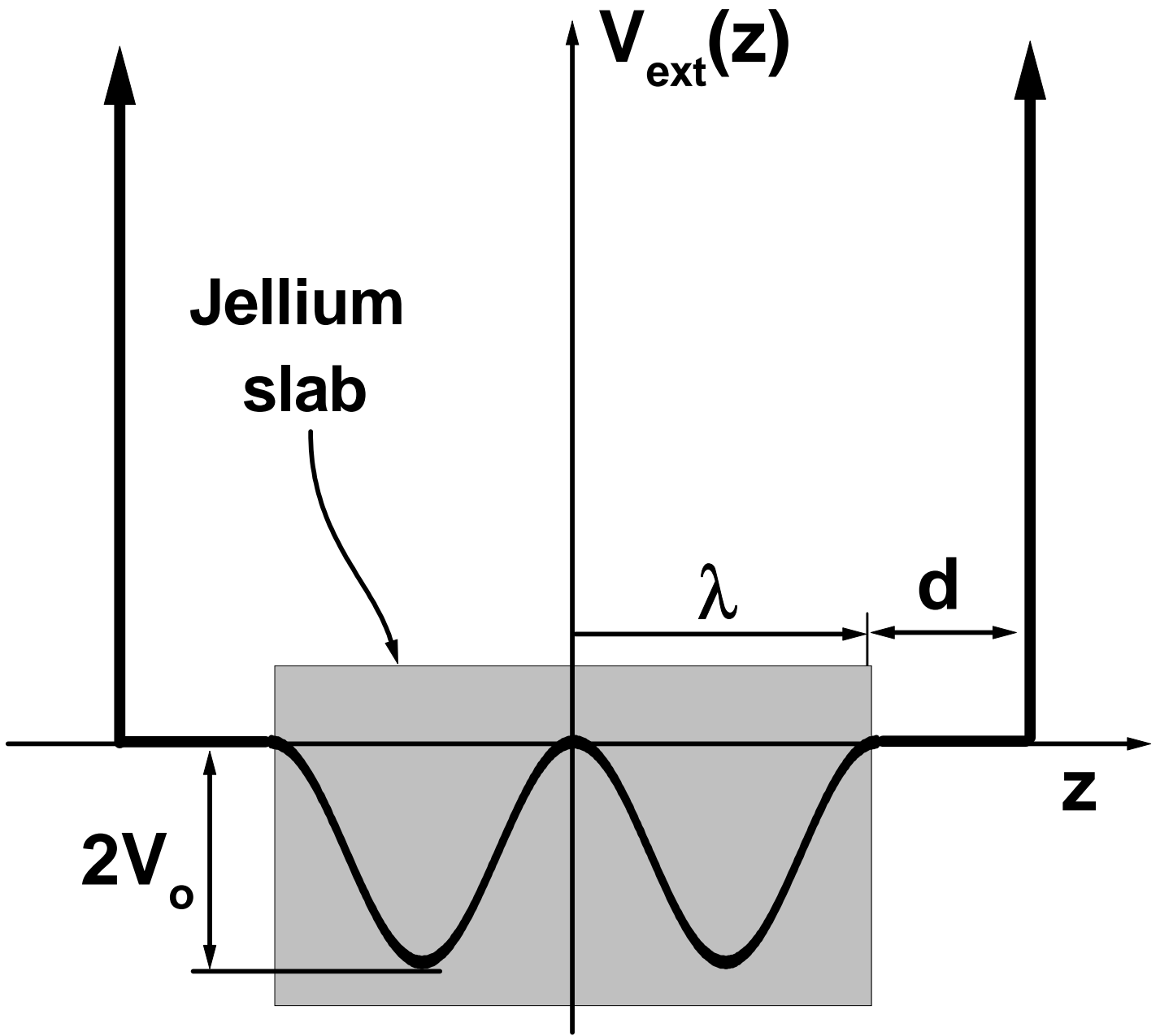
FIG. 5. Exchange-energy per particle as a function of the potential modulation. Full and dashed lines are our XX ( $\varepsilon_x^{XX}$ ) and LDA ( $\varepsilon_x^{LDA}$ ) results, respectively. Discrete points are VMC data from Ref. 9.

TABLES

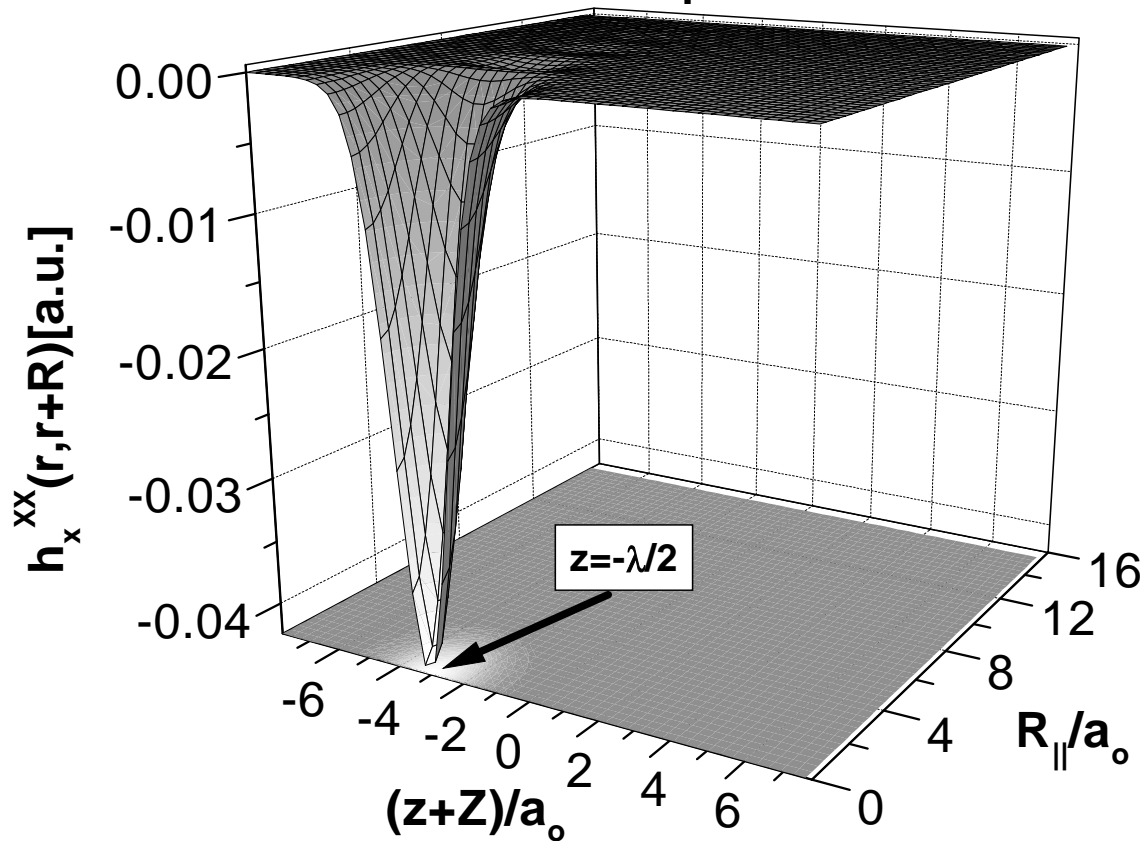
TABLE I. Exchange energy (hartrees) per particle from three different methods: XX-DFT ( $\varepsilon_x^{XX}$ ), LDA-DFT ( $\varepsilon_x^{LDA}$ ), and VMC ( $\varepsilon_x^{VMC}$ , from Ref. 23).

$q/k_F^0$	$\varepsilon_x^{XX}$	$\varepsilon_x^{LDA}$	$\varepsilon_x^{VMC}$	$\varepsilon_x^{XX} - \varepsilon_x^{VMC}$	$\varepsilon_x^{XX} - \varepsilon_x^{LDA}$
1.11	-0.2911	-0.2795	-0.2930	0.0019	-0.0116
1.55	-0.2739	-0.2687	-0.2756	0.0017	-0.0052
2.17	-0.2469	-0.2508	-0.2534	0.0065	+0.0039

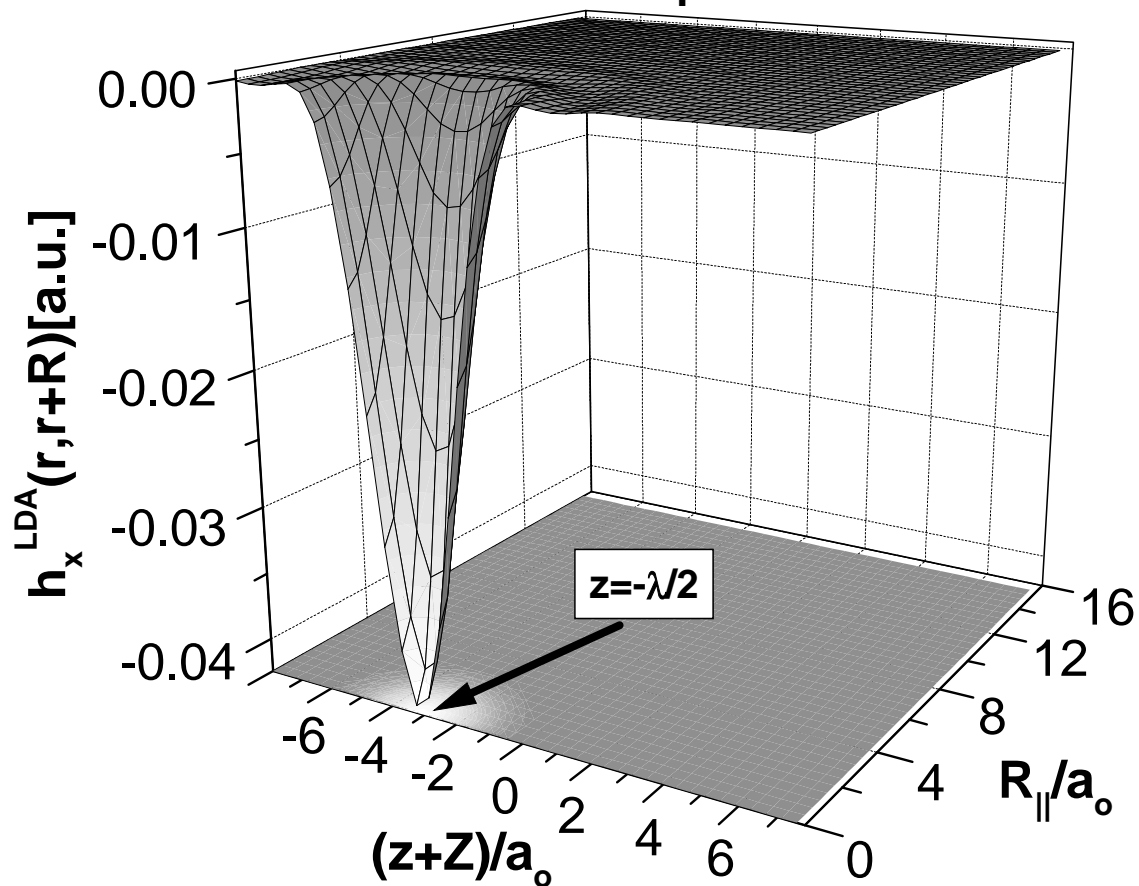
FIGURE 1



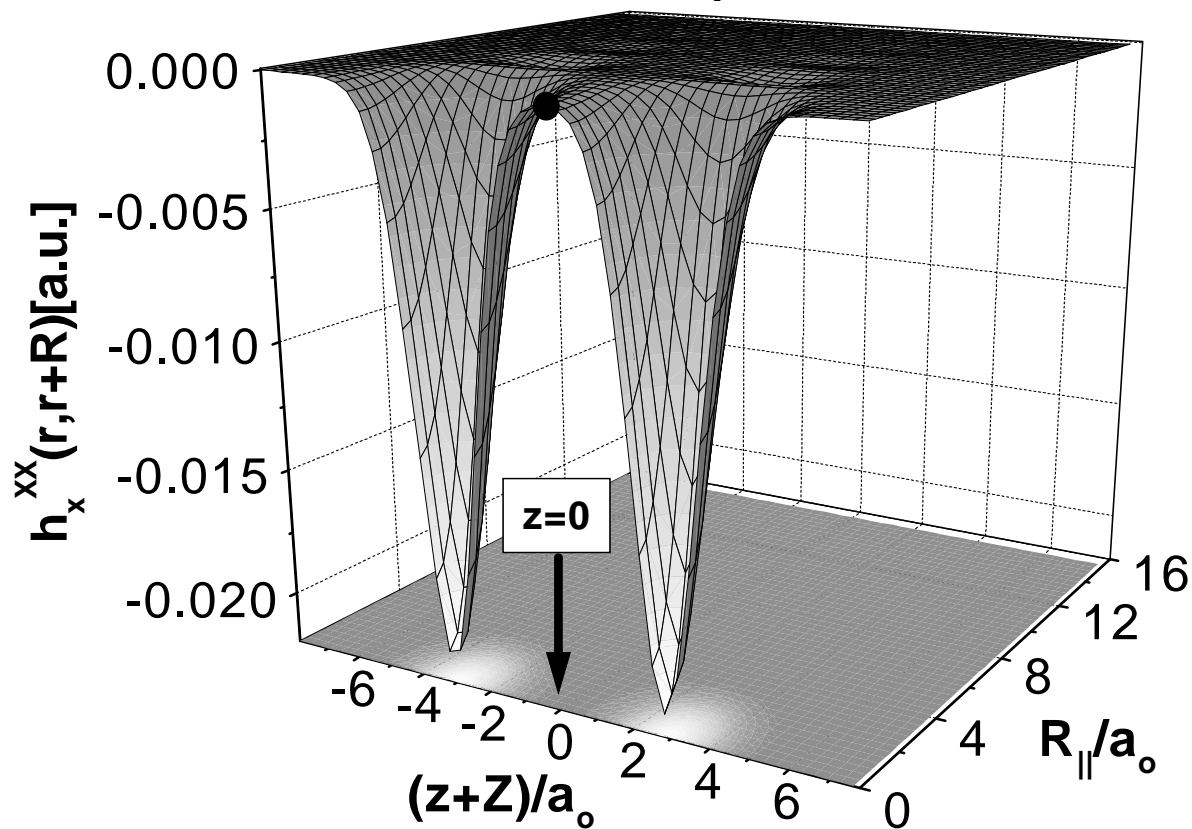
**XX,q/k<sub>F</sub><sup>0</sup>=1.11**



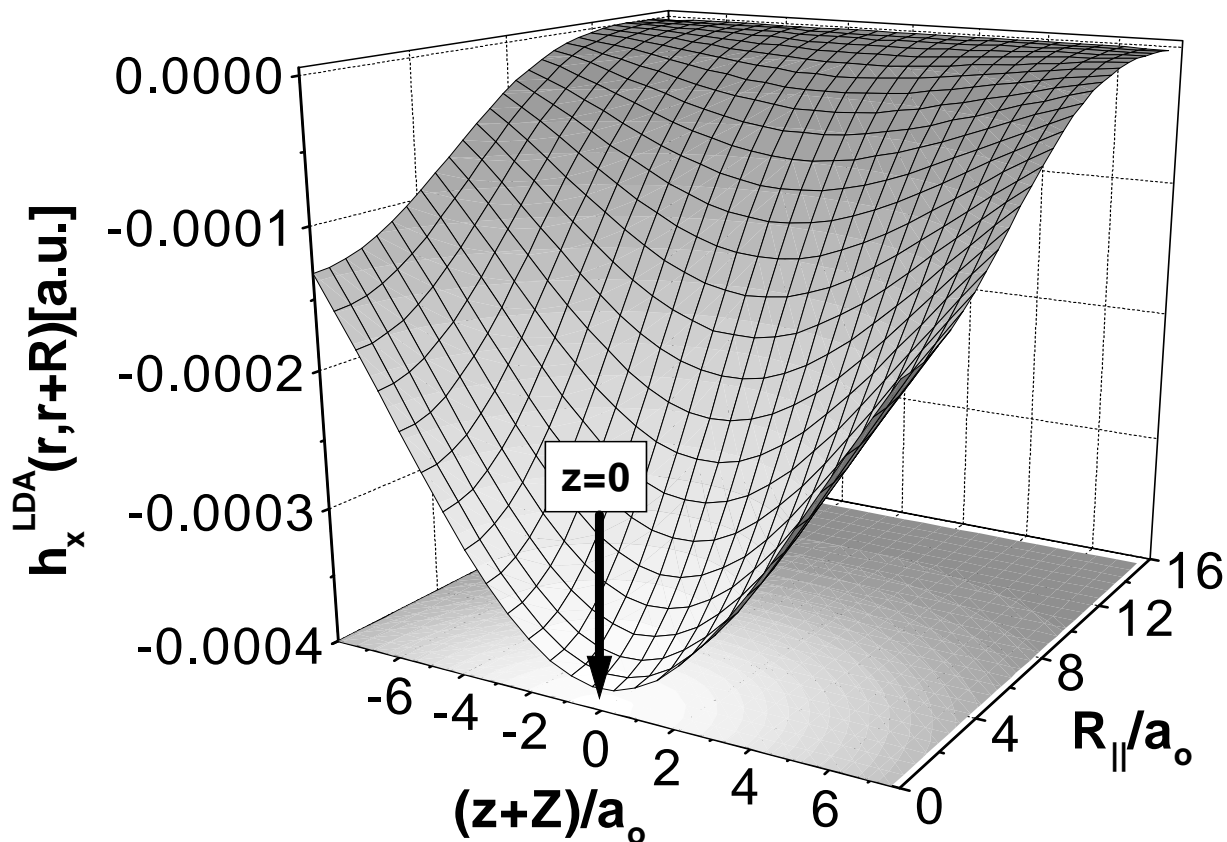
**LDA,q/k<sub>F</sub><sup>0</sup>=1.11**



**XX,q/k  $F_F^0=1.11$**



**LDA,q/k  $F_F^0=1.11$**





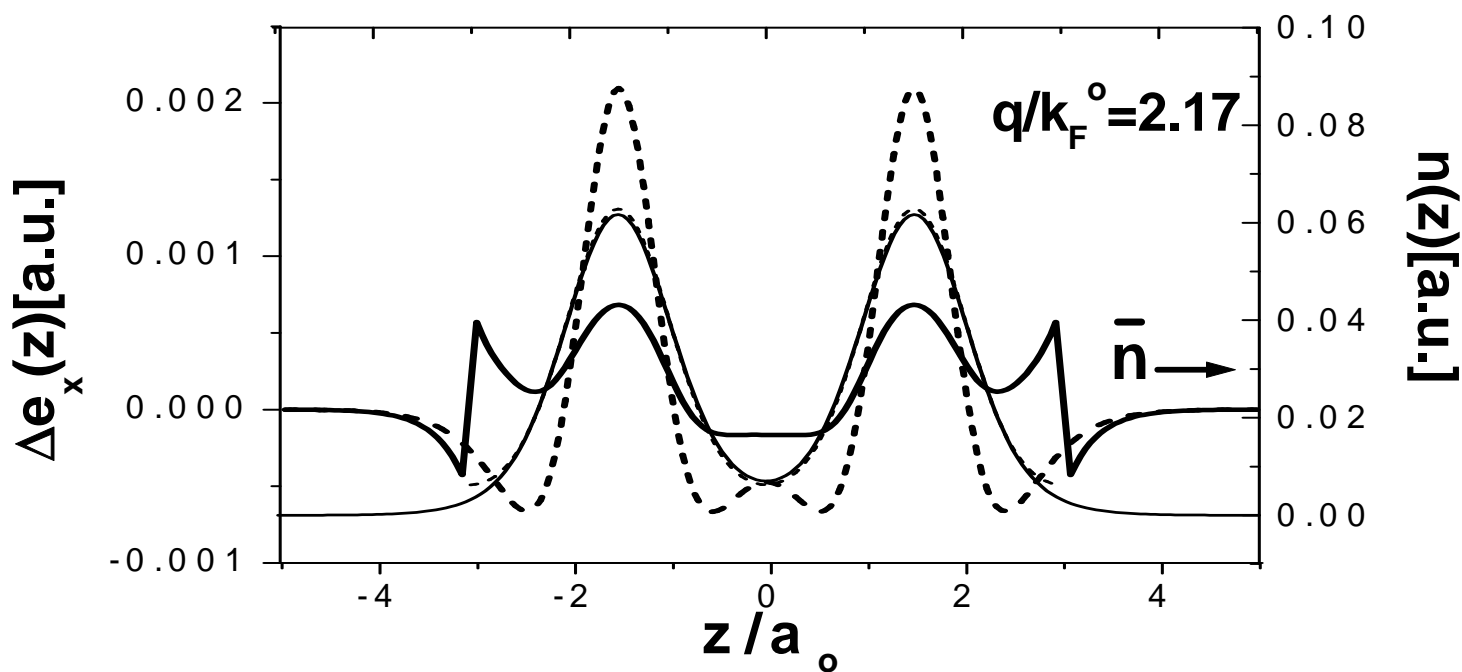
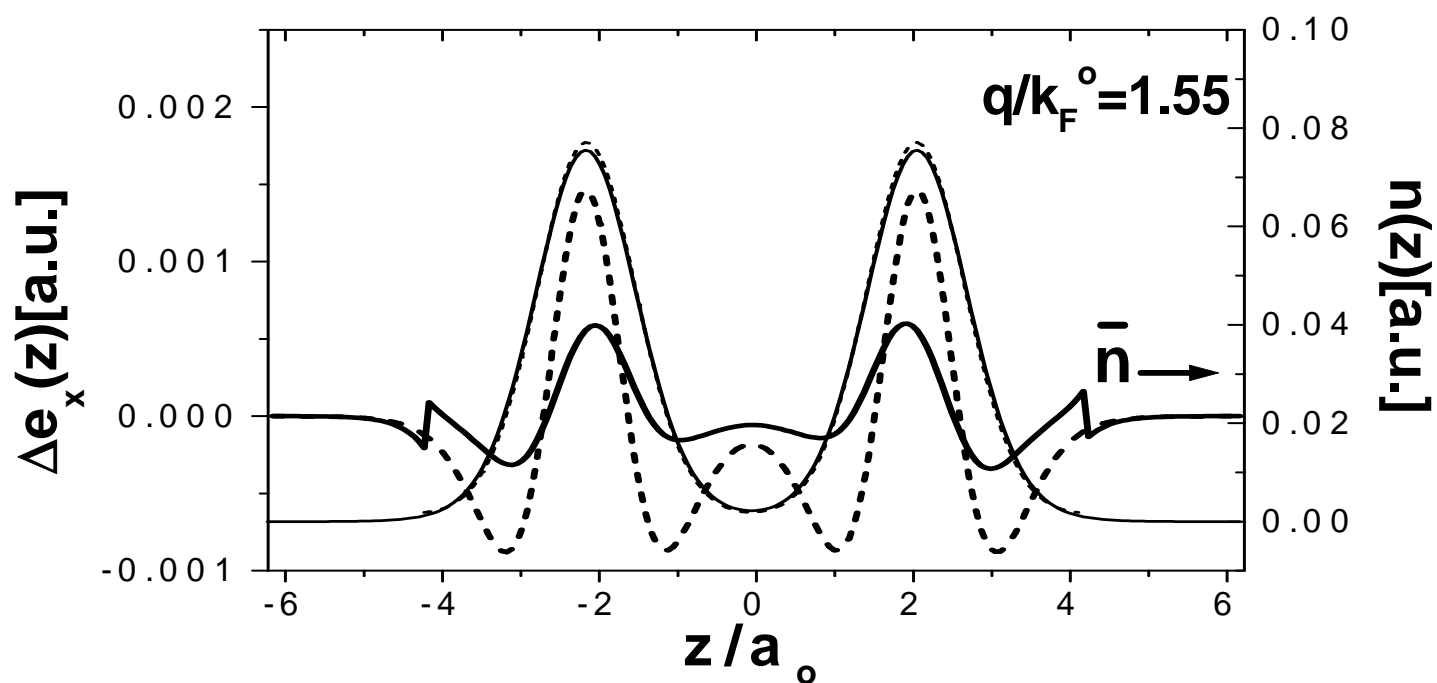
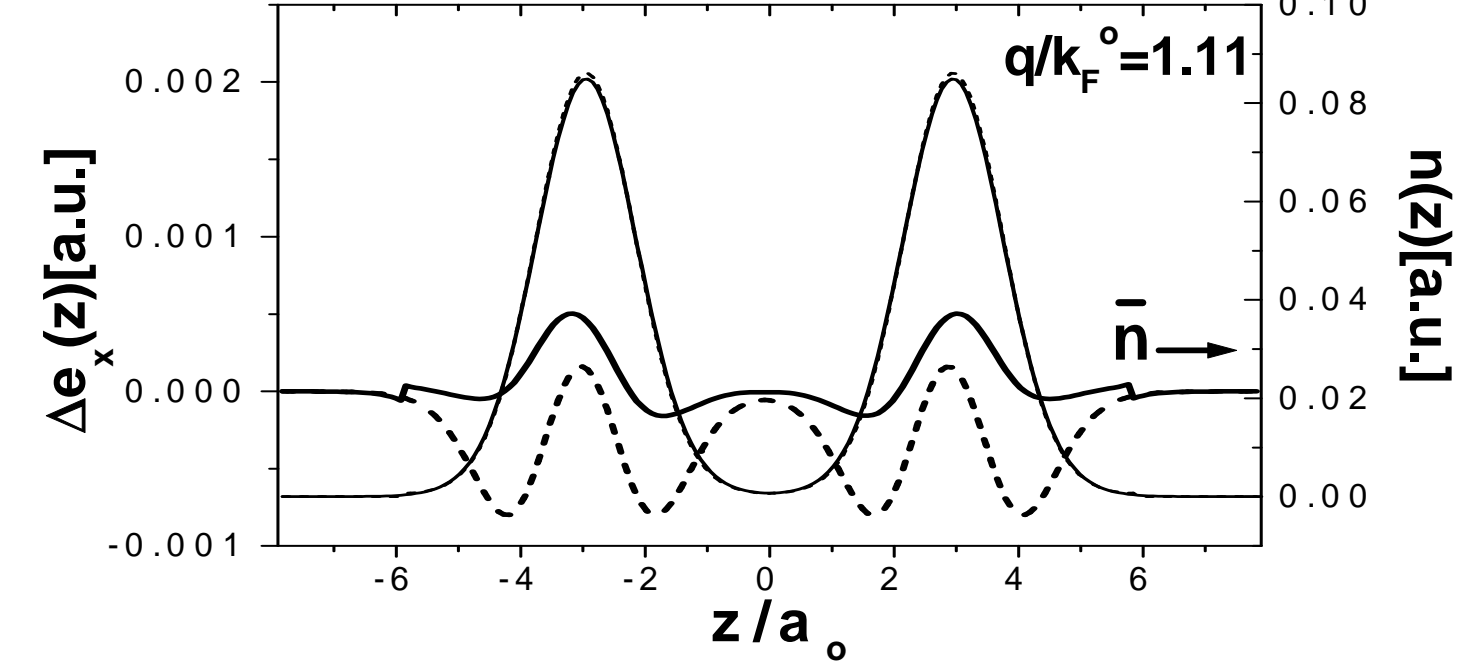


# FIGURE 5

